

804 **Chapter 3**
805 **Classical Cyclotron**

806 **Abstract** This tutorial is an introduction to the classical cyclotron, with hints at
807 spin dynamics, hands-on: by numerical simulation. It begins with a brief reminder
808 of the historical context, and then introduces the theoretical material needed for the
809 simulation exercises, which follow. Basic charged particle optics and acceleration
810 concepts are addressed, including
811 - closed orbit in a cyclic accelerator,
812 - weak focusing in a dipole magnet,
813 - periodic transverse motion,
814 - revolution period and isochronism,
815 - voltage gap and resonant acceleration,
816 - the cyclotron equation.
817 Simulations require only three optical elements, used throughout, namely: TOSCA,
818 for handling field maps; DIPOLE, an analytical model of the field in a dipole
819 magnet; and CAVITE, an oscillating voltage gap. Simulations also introduce to
820 the default output listing zgoubi.res, to optional output files such as zgoubi.plt,
821 zgoubi.CAVITE.out, zgoubi.MATRIX.out and other similar zgoubi.*.out output files
822 aimed at data post-treatment, including producing graphs. Additional keywords are
823 introduced, including FAISCEAU which allows logging local particle coordinates in
824 zgoubi.res, FAISTORE which logs local particle coordinates in a user defined file,
825 usually for further external data treatment or plotting, MARKER, the 'system call'
826 command SYSTEM, the REBELOTE 'do loop', and some more. Spin motion will
827 be solved as well, this will require introducing SPNTRK, a request to do so while
828 raytracing, and SPNPRT which prints out spin vector components to zgoubi.res.

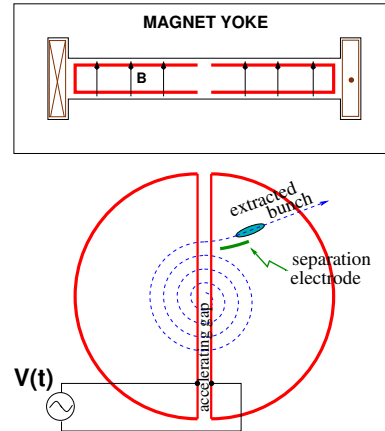
829 **Notations used in the Text**

$B; B_0$	field value; at reference radius R_0
$\mathbf{B}; B_R; B_y$	field vector; radial component; axial component
$B\rho = p/q$	particle rigidity
$C; C_0$	orbit length, $C = 2\pi R$; reference, $C_0 = 2\pi R_0$
E	particle energy
$f_{rf}; h$	RF frequency; RF harmonic number
$k = \frac{R}{B} \frac{dB}{dR}$	radial field index
$m; m_0; M$	mass; rest mass; in units of MeV/c^2
$\mathbf{p}; p; p_0$	particle momentum vector; its modulus; reference
q	particle charge
830 $R; R_0; R_E$	orbital radius; reference radius $R(p_0)$; at energy E
s	path variable
$\mathbf{v}; v$	particle velocity vector; its modulus
$V(t); \hat{V}$	oscillating voltage; its peak value
x, x', y, y'	radial and axial coordinates in the moving frame [$(*)' = d(*)/ds$]
$\beta = v/c; \beta_0; \beta_s$	normalized particle velocity; reference; synchronous
$\gamma = E/m_0$	Lorentz relativistic factor
$\Delta p, \delta p$	momentum offset
ϵ_u	Courant-Snyder invariant (u: x, r, y, l, Y, Z, s, etc.)
ϕ	RF phase at particle arrival at the voltage gap

831 **Introduction**

832 The cyclotron is the first cyclic accelerator. The concept: resonant acceleration of particles circling in a uniform magnetic field, goes back to the late 1920s [1]. The

Fig. 3.1 A sketch of the classical cyclotron. In the uniform magnetic field between two circular poles (top) an ion spirals out (bottom). A double-dee (or a single-dee facing a slotted electrode) forms a gap to which a fixed-frequency oscillating voltage $V(t)$ is applied. Its oscillation frequency is a harmonic of the revolution frequency. Particles experiencing proper voltage phase at the gap are accelerated. A septum electrode allows bunch extraction



833 first cyclotron was constructed at Berkeley, acceleration of H_2^+ hydrogen ions to
 834 80 keV [2] was achieved in 1931. The apparatus used a single dee vis-à-vis a slotted
 835 electrode forming a voltage gap, the ensemble housed in a 5 inch diameter vacuum
 836 chamber and placed in the 1.3 Tesla field of an electromagnet (Fig. 3.1). A ≈ 12 MHz
 837 vacuum tube oscillator a 1 kVolt peak gap voltage.

838 The goal foreseen in developing this technology was the acceleration of protons
 839 to MeV kinetic energy range for the study of atom nucleus - and in background a
 840 wealth of potential applications. An 11 inch cyclotron delivering a $0.01 \mu A H_2^+$ beam
 841 at 1.22 MeV [3], and then a 27 inch cyclotron reaching 6 MeV (Fig. 3.2), followed [4].
 842 In the wake of Cockcroft and Walton first artificial disintegration experiment, targets
 843 were mounted at the periphery of the 11 inch cyclotron, disintegrations were observed
 844 in 1932. And in 1933: *'The neutron had been identified by Chadwick in 1932. By*
 845 *1933 we were producing and observing neutrons from every target bombarded by*
 846 *deuterons.* " [4, M.S. Livingston,p. 22].

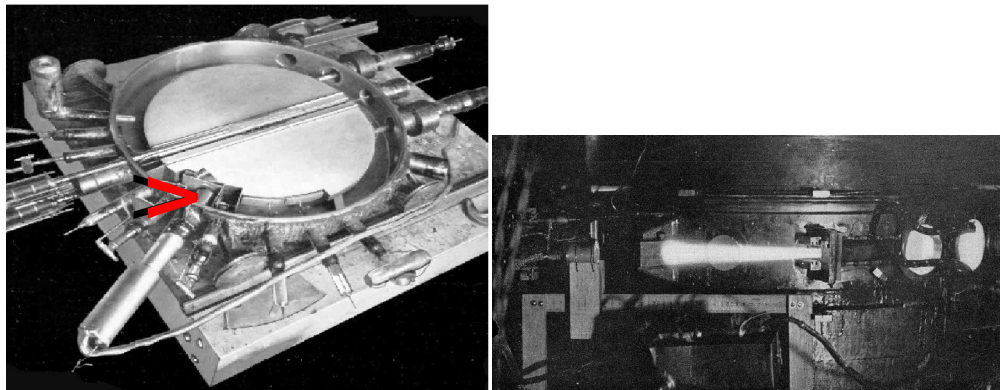


Fig. 3.2 Berkeley 27 inch cyclotron, first operated in 1934, accelerated deuterons up to 6 MeV. Left: a double-dee (seen in the vacuum chamber, cover off), 22 inch diameter, creates an accelerating gap: 13 kV, 12 MHz radio frequency voltage is applied for deuterons for instance (through two feed lines seen on the right). This apparatus was dipped in the 1.6 Tesla dipole field of a 27 in diameter (75 ton) electromagnet. A slight decrease of the dipole field with radius, from the center of the dees, assured vertical beam focusing. Particles spiral out from the center of the dees to the rim (where they strike a target, seen at the bottom on the left - arrow). Right: ionization of the air by the extracted beam (1936); the view also shows the vacuum chamber squeezed between the pole pieces of the electromagnet

847 The scope with accelerated beams from cyclotrons was broad: *"At this time*
 848 *biological experiments were started. I can recall the first time that a mouse was*
 849 *irradiated with neutrons. We put the mouse in a little cage and stuck him up on the*
 850 *side of the cyclotron tank and left him there for a while. Of course, nothing happened*
 851 *because [etc.]"* [4, McMillan,p.26]; and *"Also at about this same time the first*
 852 *radioactive tracer experiments on human beings were tried"* [op.cit.]; *"[...] simple*
 853 *beginnings of therapeutic use, coming a little bit later, in which neutron radiation was*
 854 *used, for instance, in the treatment of cancer. These things have gone on and built up*

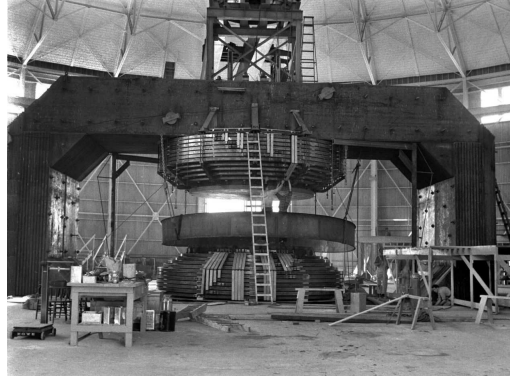


Fig. 3.3 Berkeley 184 in cyclotron. It was modified into a synchrocyclotron in 1946

855 *so that there's now a whole field*" [op.cit.]; and *"Another highlight from 1936 was the*
 856 *first time that anyone tried to make artificially a naturally occurring radionuclide."*
 857 (a bismuth isotope) [op.cit.]. The period also saw beam extraction developments
 858 (Fig. 3.2). Cyclotrons were constructed in many laboratories worldwide, from the
 859 early 1930s, following Berkeley demonstration.

860 *Limitation in energy*

861 An advanced theoretical understanding of the cyclotron more or less took until the
 862 mid-1930s, ending up with two news, a bad one and a good one, bad one first:

863 (i) the energy limitation, a consequence of the loss of isochronism resulting from
 864 the relativistic increase of the ion mass: "[...] *it seems useless to build cyclotrons of*
 865 *larger proportions than the existing ones [...] an accelerating chamber of 37 in radius*
 866 *will suffice to produce deuterons of 11 MeV energy which is the highest possible*
 867 *[...]*" [5] (related simulations will conclude this Chapter, "Classical Cyclotron"), or
 868 in a different form: *"If you went to graduate school in the 1940s, this inequality*
 869 *($-1 < k < 0$) was the end of the discussion of accelerator theory*" [6].

870 The good news next:

871 (ii) the overcoming of that relativistic limit, due to L.H. Thomas in 1938 [7] - it
 872 took a few years though, to see practical effects.

873 Classical cyclotron technology has been in use for some time up to the few tens
 874 of MeV/u that it allows (Fig. 3.4), for such applications as neutron production for
 875 material science, radio-isotope production for medicine, injector stages in cyclotron
 876 complex facilities [9]. However with the progress in magnet computation tools and
 877 magnet fabrication (including permanent magnet techniques [10]), and the progress
 878 in computational speed and beam dynamics simulations (which includes accurate
 879 raytracing, as concerned in the present opus), the azimuthally varying field (AVF,
 880 or Thomas' [7]) cyclotron, much more performing, comes out to be essentially as
 881 simple and has in a general manner prevailed (Fig. 3.4).

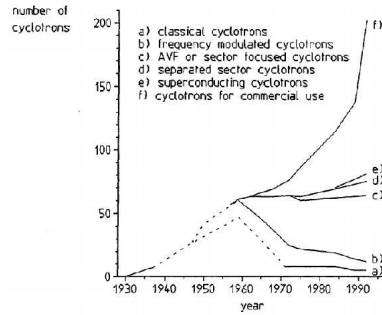
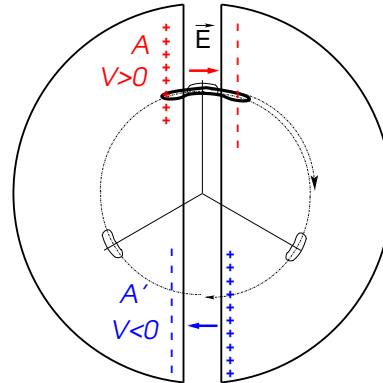


Fig. 3.4 Evolution of cyclotron species, over the years [8, Fig. 8]

882 **3.1 Theory, Basic Concepts**

883 The cyclotron was conceived as a means to overcome the inconvenience of using a
 884 long series of high voltage electrodes in a linear layout, by, instead, repeated re-
 885 circulation using a magnetic field, for incremental, resonant, energy gain through
 a single accelerating gap. This gap is formed by a pair of cylindrical electrodes,

Fig. 3.5 Resonant acceleration: a positive ion bunch meets an accelerating field **E** across gap A, at time *t*; it meets again, half a revolution later, at time $t + T_{rev}/2$, an accelerating field across gap A', and so on so forth. In this $h = 1$ configuration, one bunch (and only one) over a turn is in synchronism with the accelerating phase of the oscillating voltage, at both gaps. Higher *h* allows more bunches: the next possibility with two dees would be $h=3$, and three stable bunches at 120 degrees from one another (thin contours) over a turn



886 “dees” (Fig. 3.5) which are applied a fixed frequency oscillating voltage, generated
 887 using a radio transmitter. The dees are placed in a uniform magnetic field which
 888 causes the ion bunches to follow, as they are accelerated, a piecewise-circular motion
 889 with increasing radius, normal to the field, more or less in phase with the voltage
 890 oscillation. An oscillating voltage is necessary as a DC voltage gap (a conservative
 891 field) in a circular accelerator can not yield energy gain: with the advent of resonant
 892 acceleration in the cyclotron and the development of cyclic accelerators in the hori-
 893 zon, it is interesting to note in passing that it is not possible to accelerate a particle
 894

895 traveling on a closed path using an electrostatic field ($\mathbf{E} = -\mathbf{grad}V(\mathbf{R}, t)$ derives
 896 from a scalar potential), as the work by $\mathbf{F} = q\mathbf{E}$ only depends on the initial and final
 897 states, it does not dependent on the path followed (Fig. 3.6), which can be written

$$W = \int_P^Q \mathbf{F}.ds = -q \int_P^Q \mathbf{grad}V.ds = -q(V_Q - V_P) \quad (3.1)$$

898 On a closed path: $\oint \mathbf{F}.ds = 0$, the force is conservative, no work is performed,
 899 consequence: a DC voltage gap in a circular machine does not yield energy gain.

900 Instead, the work of a force of induction origin, where $\mathbf{E} = -\partial\mathbf{A}/\partial t$ arises from
 901 the variation of a magnetic flux ($\mathbf{B} = \mathbf{curl}\mathbf{A}$, \mathbf{A} a vector potential), may be non-zero
 902 on a closed path. This is achieved for instance using a radio-frequency system which
 903 feeds an oscillating voltage across a gap, $V(t) = \hat{V} \sin(\omega_{rf}t + \phi)$ (Fig. 3.7).

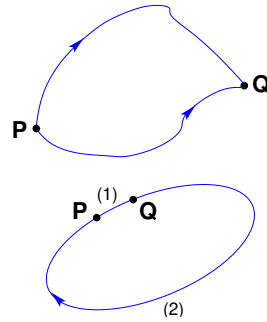


Fig. 3.6 Top: the work of the electrostatic force $\mathbf{F} = q\mathbf{E}$ is $W = \int_P^Q \mathbf{F}.ds = -q(V_Q - V_P)$. Bottom: over closed path, the particle loses along (2) the energy gained along (1)

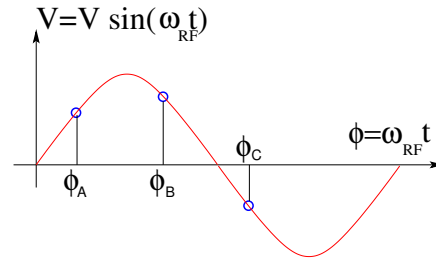


Fig. 3.7 A particle which reaches the double-dee gap at the RF phase $\omega_{rf}t = \phi_A$ or $\omega_{rf}t = \phi_B$ is accelerated. If it reaches the gap at $\omega_{rf}t = \phi_C$ it is decelerated

904 As an accelerated bunch spirals outward in a uniform magnetic field, the increase
 905 in the distance it travels over a turn is compensated by its velocity increase: in
 906 the non-relativistic approximation ($\beta \ll 1$), the revolution period T_{rev} increases
 907 only slowly with energy; with appropriate voltage frequency $f_{rf} \approx h/T_{rev}$ revolution
 908 motion and RF can be maintained in sufficiently close synchronism, $T_{rev} \approx hT_{rf}$, that
 909 the bunch will transit the accelerating gaps (Fig. 3.5) during the accelerating phase
 910 of the oscillating $V(t)$ (Fig. 3.7).

911 The orbital motion quantities: radius R , field B , particle rigidity BR , revolution
912 frequency $f_{\text{rev}} = \omega_{\text{rev}}/2\pi$, satisfy

$$BR = \frac{p}{q}, \quad 2\pi f_{\text{rev}} = \frac{v}{R} = \frac{qB}{m} = \frac{qB}{\gamma m_0} \quad (3.2)$$

These relationships hold at all γ , from $v \ll c$ ($\gamma \approx 1$, domain of the *classical* cyclotron) to $\gamma > 1$ (domain of the *isochronous* cyclotron). To give an idea of the revolution frequency, in the limit $\gamma = 1$ one has

$$\frac{f_{\text{rev}}}{B} = \frac{q}{2\pi m} = 15.25 \text{ MHz/T} \quad \text{for protons.}$$

913 The RF frequency $f_{\text{rf}} = \omega_{\text{rf}}/2\pi$ is constant in a cyclotron, whereas the revolution
914 period slowly increases with energy (Sec. 3.1.3). In the classical cyclotron f_{rf} is set,
915 by design, equal to hf_{rev} for an intermediate energy taken along the acceleration
916 cycle. The energy gain, or loss, by the particle when transiting the gap is

$$\Delta W = q\hat{V} \sin \phi(t) \quad \text{with } \phi(t) = \omega_{\text{rf}}t - \omega_{\text{rev}}t + \phi_0 \quad (3.3)$$

917 with ϕ its phase with respect to the RF signal at the gap (*e.g.*, ϕ_A , ϕ_B or ϕ_C in
918 Fig. 3.7) and ϕ_0 the value at $t = 0$, $\omega_{\text{rev}}t$ the orbital angle advance.

Fixed-frequency acceleration requires the RF and cyclotron frequencies to be matched to one another. However the relativistic increase of the mass upon velocity increase causes the revolution period to increase with momentum: in $T_{\text{rev}} = 2\pi m/qB$, B is almost constant and m increases, resulting in a turn-by-turn

$$\frac{\Delta T_{\text{rev}}}{T_{\text{rev}}} = \gamma - 1$$

919 The mis-match between the accelerating RF and cyclotron frequencies is a
920 turn-by-turn cumulative effect and sets a limit to the tolerable isochronism defect,
921 $\Delta T_{\text{rev}}/T_{\text{rev}} \approx 2 - 3\%$, or highest velocity $\beta = v/c \approx 0.22$. This results for instance in
922 a practical limitation of the “classical cyclotron” to an upper ≈ 25 MeV for protons,
923 and ≈ 50 MeV for D and α particles.

924 To conclude on these basis concepts regarding acceleration, multiple accelerating
925 gap structures is part of the evolutions of the classical cyclotron, where a “D” is
926 rather a “ Δ ” pattern, and towards high RF frequency harmonic. An example among
927 many others is, as an illustration, GANIL C0 injector with its 4 accelerating gaps
928 and h=4 and h=8 RF operation [9].

929 3.1.1 Fixed-Energy Orbits, Revolution Period

930 The differential equations of particle motion are established in the Serret-Frénet
931 frame, Sec. 3.1.2, however, some basic geometrical properties can be derived in the

932 laboratory frame, as follows. In the laboratory frame (O;x,y,z), with (O;x,z) the bend
 933 plane, assume $\mathbf{B}|_{y=0} = \mathbf{B}_y$. A particle is launched from the origin with a velocity
 934 $\mathbf{v} = (v \sin \alpha, 0, v \cos \alpha)$ at an angle α from the longitudinal axis z.

935 Solving

$$m\dot{\mathbf{v}} = q\mathbf{v} \times \mathbf{B} \quad (3.4)$$

936 with $\mathbf{v} = (\dot{x}, \dot{y}, \dot{z})$, $\mathbf{B} = (0, B_y, 0)$ yields the parametric equations of motion

$$\begin{cases} x(t) = \frac{v}{\omega_{\text{rev}}} \cos(\omega_{\text{rev}}t - \alpha) - \frac{v \cos \alpha}{\omega_{\text{rev}}} \\ z(t) = \frac{v}{\omega_{\text{rev}}} \sin(\omega_{\text{rev}}t - \alpha) + \frac{v \sin \alpha}{\omega_{\text{rev}}} \\ y(t) = \text{constant} \end{cases} \quad (3.5)$$

937 which results in

$$\left(x + \frac{v \cos \alpha}{\omega_{\text{rev}}}\right)^2 + \left(z - \frac{v \sin \alpha}{\omega_{\text{rev}}}\right)^2 = \left(\frac{v}{\omega_{\text{rev}}}\right)^2 \quad (3.6)$$

a circular trajectory of radius $R = p/qB$ centered at $x = -v \cos \alpha / \omega_{\text{rev}}$, $z = v \sin \alpha / \omega_{\text{rev}}$, revolution period

$$T_{\text{rev}} = \frac{2\pi}{\omega_{\text{rev}}} = \frac{2\pi m}{qB}$$

938 *Cyclic motion* - Horizontal motion in uniform field has no privileged reference orbit:
 939 for a given momentum, the initial radius and velocity vector define a particular closed,
 940 circular orbit. A particle launched with an axial velocity component v_y on the other
 941 hand, drifts vertically linearly with time, as there is no axial restoring force. The next
 942 Section will investigate the necessary field property, absent in our simplified field
 943 model so far, proper to ensure confinement of the multiturn 6-dimensional periodic
 944 motion in the vicinity of the median plane of the cyclotron dipole magnet.

945 3.1.2 Weak Focusing, Transverse Motion

946 In the lower energy (smaller radius) accelerated turns in a classical cyclotron, the
 947 electric field in the accelerating gap contributes proper transverse focusing so that
 948 the magnet gap can be designed parallel (an example can be found in Ref. [9]). In
 949 very low energy applications even, extraction energy in the tens of keV/u range where
 950 electric fields are still effective, flat magnetic field with uniformity $dB/B < 10^{-4}$
 951 can be achieved over the (reduced) extent of the cyclotron orbit and maintains proper
 952 isochronism. Beyond this low energy region however, at greater radius, a magnetic
 953 field gradient must be introduced, field decreasing with R, by shaping the magnet
 954 poles, to ensure proper vertical focusing. Note that because of the field decreases

955 with R in a parallel gap, as discovered *a posteriori*, the very first cyclotrons were
 956 working [11]. This section introduces to these magnetic focusing principles.

957 In the following, $B_R(R)$, $B_y(R)$ denote the radial and axial components of the
 958 magnetic field at radius R . Median-plane symmetry of the field is assumed, thus
 959 $B_R|_{y=0} = 0$ at all R (Fig. 3.8). Particle coordinates are defined in the Serret-Frénet
 960 frame $(O; s, x, y)$, moving along the R_0 radius reference orbit (the origin O is at the
 961 location of the reference particle, s axis tangent to the reference orbit, x axis radial,
 962 y axis normal to the bend plane, Fig. 3.9). The radial excursion of a particle with
 963 respect to the reference orbit writes

$$x(t) = R(t) - R_0 \ll R_0 \quad (3.7)$$

964 Considering small radial and axial excursions from $(R = R_0, y = 0)$, a Taylor
 965 expansion of the magnetic field can be introduced,

$$\begin{aligned} B_y(R_0 + x) &= B_y(R_0) + x \left. \frac{\partial B_y}{\partial R} \right|_{R_0} + \frac{x^2}{2!} \left. \frac{\partial^2 B_y}{\partial R^2} \right|_{R_0} + \dots \approx B_y(R_0) + x \left. \frac{\partial B_y}{\partial R} \right|_{R_0} \\ B_R(0 + y) &= y \left. \frac{\partial B_R}{\partial y} \right|_0 + \frac{y^3}{3!} \left. \frac{\partial^3 B_R}{\partial y^3} \right|_0 + \dots \approx y \left. \frac{\partial B_y}{\partial R} \right|_{R_0} \\ &= \left. \frac{\partial B_y}{\partial R} \right|_{R_0} y \end{aligned} \quad (3.8)$$

966 Using this approximation, the differential equations of motion in the moving frame
 967 can be written under the form, linear in x and y ,

$$\begin{aligned} F_x = m\ddot{x} &= -qvB_y(R) + \frac{mv^2}{R_0 + x} \approx -qv \left(B_y(R_0) + \left. \frac{\partial B_y}{\partial R} \right|_{R_0} x \right) + \frac{mv^2}{R_0} \left(1 - \frac{x}{R_0} \right) \\ &\rightarrow m\ddot{x} = -\frac{mv^2}{R_0^2} \left(\frac{R_0}{B_0} \left. \frac{\partial B_y}{\partial R} \right|_{R_0} + 1 \right) x \\ F_y = m\ddot{y} &= qvB_R(y) = qv \left. \frac{\partial B_R}{\partial y} \right|_{y=0} y + \text{higher order} \rightarrow m\ddot{y} = qv \left. \frac{\partial B_y}{\partial R} \right|_{R_0} y \end{aligned} \quad (3.9)$$

968 Note $B_y(R_0) = B_0$ and introduce
 969

$$\omega_R^2 = \omega_{\text{rev}}^2 \left(1 + \frac{R_0}{B_0} \left. \frac{\partial B_y}{\partial R} \right|_{R_0} \right), \quad \omega_y^2 = -\omega_{\text{rev}}^2 \frac{R_0}{B_0} \left. \frac{\partial B_y}{\partial R} \right|_{R_0} \quad (3.10)$$

970 equations 3.9 can thus be written under the form

$$\ddot{x} + \omega_R^2 x = 0 \quad \text{and} \quad \ddot{y} + \omega_y^2 y = 0 \quad (3.11)$$

971 A restoring force (linear terms in x and y , Eq. 3.11) arises from the radially varying
 972 field, characterized by a field index

Fig. 3.8 Axial motion stability requires proper shaping of field lines: B has to decrease with radius. The Laplace force pulls a charge at I (velocity pointing out of the page) toward the median plane. Increasing the field gradient (k closer to -1 , gap opening up faster) increases the focusing

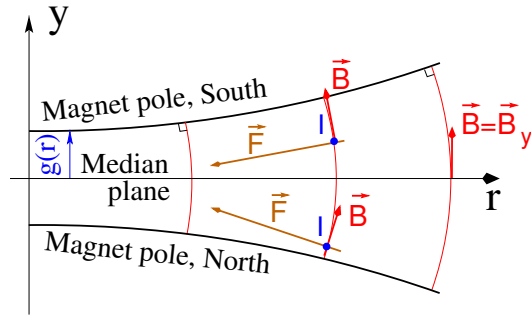


Fig. 3.9 Radial motion stability in an axially symmetric structure. Arrowed arcs are trajectories of particles with momentum $p=mv$. Dashed arcs are centered at C , center of the cyclotron. The resultant $F_i = -qvB + mv^2/r$, is zero at I : $B_0R_0 = mv/q$. The resultant at i is toward I if $qvB_i < mv^2/R_i$, i.e. $B_iR_i < mv/q$; the resultant at e is toward I if $qvB_e > mv^2/R_e$, i.e. $B_eR_e > mv/q$

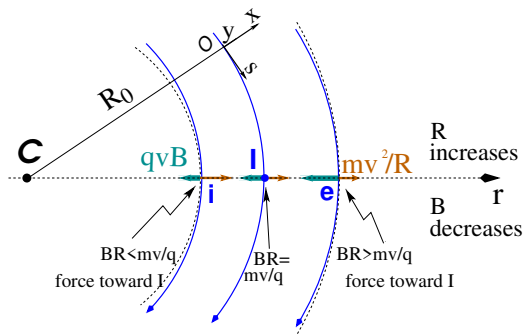
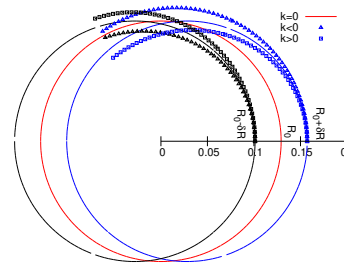


Fig. 3.10 Geometrical focusing: in a flat field, $k=0$, the two circular trajectories at $r = R_0 \pm \delta R$ (solid lines) undergo exactly one oscillation around the reference orbit $r = R_0$. A positive k increases the convergence (square markers - but then the vertical motion diverges from the median plane), a negative k decreases the convergence (triangles)



$$k = \frac{R_0}{B_0} \left. \frac{\partial B_y}{\partial R} \right|_{R=R_0, y=0} \quad (3.12)$$

973 and adds in the radial motion to the focusing due to the curvature (the term “1” in
974 ω_R^2 , Eq. 3.10).

975 *Axial stability* in a cyclotron requires a restoring force directed toward the median
976 plane. Referring to Fig. 3.8, this means $F_y = -ay$ (with the a factor some positive
977 quantity) and thus $B_R < 0$, at all $(r, y \neq 0)$. This is achieved by designing a guiding
978 field which decreases with radius, $\frac{\partial B_R}{\partial y} < 0$. Referring to Eq. 3.12 this translates into
979 $k < 0$.

980 *Radial stability* in a constant field is a geometrical property, resulting from the
981 curvature of the trajectory (Fig. 3.10). In a weakly decreasing field $B(R)$ on the other
982 hand, a particle with momentum $p = mv$ sinusoidal around the R_0 -radius reference
983 circle experiences in the Serret-Frénet frame a total force $F_t = -qvB + m\frac{v^2}{r}$ (Fig. 3.9)
984 of which the (outward) component $f_c = m\frac{v^2}{r}$ decreases with r at a higher rate than
985 the decrease of the Laplace (inward) component $f_B = -qvB(r)$. In other words, radial
986 stability requires BR to increase with R , $\frac{\partial BR}{\partial R} = B + R\frac{\partial B}{\partial R} \geq 0$, this holds in particular
987 at R_0 , thus $1 + k \geq 0$.

988 The condition for transverse motion stability around the circular equilibrium orbit
989 results from these axial and radial stability conditions, namely,

$$-1 \leq k < 0 \quad (3.13)$$

Note regarding the geometrical focusing: the focal distance associated with the
curvature of a magnet of arc length \mathcal{L} is obtained by integrating $\frac{d^2x}{ds^2} + \frac{1}{R_0^2}x = 0$ and
identifying with the focusing property $\Delta x' = -x/f$, namely,

$$\Delta x' = \int \frac{d^2x}{ds^2} ds \approx \frac{-x}{R^2} \int ds = \frac{-x\mathcal{L}}{R^2}, \text{ thus } f = \frac{R^2}{\mathcal{L}}$$

990 *Isochronism*

991 The relativistic increase of the mass precludes strict isochronism: the revolution
992 frequency slowly decreases with the energy of the particle on its spiraling out
993 trajectory (Eq. 3.2). The focusing condition $-1 < k < 0$ (B decreasing with R) further
994 contributes breaking the isochronism by virtue of $\omega_{rev} \propto B$. As a consequence, the
995 phase of the oscillating voltage at arrival of a particle at the accelerating gap (the
996 so-called RF phase) changes turn after turn. This is addressed further in Sec. 3.1.3.

997 **Paraxial Transverse Coordinates**

998 Introducing the path variable, s , as the independent variable in Eq. 3.11 and using
 999 the approximation $ds \approx vdt$ (*i.e.*, neglecting the transverse velocity components), the
 1000 equations of motion in the moving frame (Eq. 3.11) take the form

$$\frac{d^2x}{ds^2} + \frac{1+k}{R_0^2}x = 0 \quad \text{and} \quad \frac{d^2y}{ds^2} - \frac{k}{R_0^2}y = 0 \quad (3.14)$$

1001 Given $-1 < k < 0$ the motion is that of a harmonic oscillator, in both planes, with
 1002 respective restoring constants $(1+k)/R_0^2$ and $-k/R_0^2$, both positive quantities. The
 1003 solution is a sinusoidal motion,

$$\begin{cases} R(s) - R_0 = x(s) = x_0 \cos \frac{\sqrt{1+k}}{R_0}(s - s_0) + x'_0 \frac{R_0}{\sqrt{1+k}} \sin \frac{\sqrt{1+k}}{R_0}(s - s_0) \\ R'(s) = x'(s) = -x_0 \frac{\sqrt{1+k}}{R_0} \sin \frac{\sqrt{1+k}}{R_0}(s - s_0) + x'_0 \cos \frac{\sqrt{1+k}}{R_0}(s - s_0) \end{cases} \quad (3.15)$$

1004

$$\begin{cases} y(s) = y_0 \cos \frac{\sqrt{-k}}{R_0}(s - s_0) + y'_0 \frac{R_0}{\sqrt{-k}} \sin \frac{\sqrt{-k}}{R_0}(s - s_0) \\ y'(s) = -y_0 \frac{\sqrt{-k}}{R_0} \sin \frac{\sqrt{-k}}{R_0}(s - s_0) + y'_0 \cos \frac{\sqrt{-k}}{R_0}(s - s_0) \end{cases} \quad (3.16)$$

1005 The dissymmetry between the two frequencies, a “1” in “ $\sqrt{1+k}$ ” compared to $\sqrt{-k}$,
 1006 stems from the geometrical focusing resulting from the curvature.

1007 Two wave numbers may be introduced,

$$\nu_R = \frac{\omega_R}{\omega_{rev}} = \sqrt{1+k} \quad \text{and} \quad \nu_y = \frac{\omega_y}{\omega_{rev}} = \sqrt{-k} \quad (3.17)$$

1008 *i.e.*, the number of sinusoidal oscillations of the paraxial motion about the reference
 1009 circular orbit over a turn, respectively radial and axial. Both are less than 1: there
 1010 is less than one sinusoidal oscillation in a revolution. In addition, as a result of the
 1011 revolution symmetry,

$$\nu_R^2 + \nu_y^2 = 1 \quad (3.18)$$

1012 Phase Space

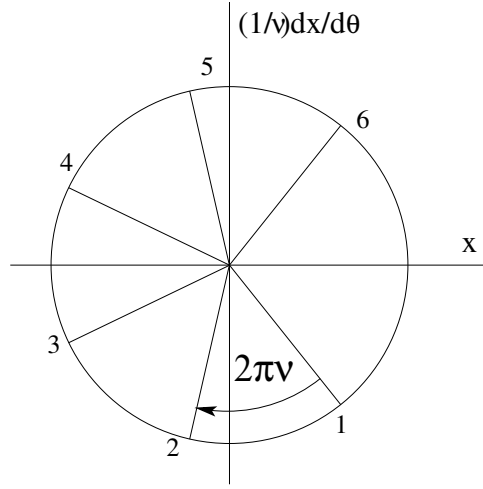
1013 Phase space at an azimuth s around the ring is a Cartesian space with, regarding
 1014 transverse particle motion, position as the horizontal axis and angle as the vertical
 1015 axis, *i.e.*, $(x(s), x'(s) = dx/ds)$ and $(y(s), y'(s) = dy/ds)$ (Eqs. 3.15 3.16), or akin
 1016 quantities, this is illustrated in Fig. 3.11.

1017 Longitudinal phase space coordinates are the RF phase ϕ (Fig. 3.7, Eq. 3.3) and
 1018 energy offset, or akin quantities.

1019 A point in phase space represents the position of a particle at azimuth s at time t .

1020 Particle motion over time depends on the field experienced and on two initial
 1021 conditions (initial position and angle, or RF phase and energy offset, ...). It is
 1022 impossible for two trajectories with different origins to coincide in phase space, at
 1023 any azimuth.

Fig. 3.11 Particle motion observed in transverse horizontal phase space at some fixed azimuth $s = R\theta_{\text{obs}}$ along the cyclotron circumference, at successive times (or turns: 1, 2, 3, ...). The horizontal axis here is $x(\theta_{\text{obs}})$, the vertical axis is $\frac{1}{v_R} \frac{dx}{d\theta} \Big|_{\theta=\theta_{\text{obs}}}$, using these coordinates the motion is on a circle of radius \hat{x} . Note that $\{x(\theta_{\text{obs}}) = \hat{x} \cos(\nu_R \theta_{\text{obs}} + \phi)$ and $\frac{1}{v_R} \frac{dx}{d\theta} \Big|_{\theta=\theta_{\text{obs}}} = -\hat{x} \sin(\nu_R \theta_{\text{obs}} + \phi)\}$ establishes that phase space motion is clockwise



1024 Off-Momentum Motion

1025 Momenta of particles that make up a bunch accelerated in a cyclotron span some
1026 extent $\pm\Delta p/p$.

In an axially symmetric structure, the equilibrium trajectory at momentum $\begin{cases} p_A \\ p_B = p_A + \Delta p \end{cases}$ is at radius $\begin{cases} R_A \text{ such that } B_A R_A = p_A/q \\ R_B \text{ such that } B_B R_B = p_B/q \end{cases}$, with $\begin{cases} B_B = B_A + \left(\frac{\partial B}{\partial x}\right)_0 + \dots \\ R_B = R_A + \Delta x \end{cases}$

On the other hand

$$B_B R_B = \frac{p_B}{q} \Rightarrow \left[B_A + \left(\frac{\partial B}{\partial x}\right)_0 \Delta x + \dots \right] (R_A + \Delta x) = \frac{p_A + \Delta p}{q} = \frac{p_A}{q} + \frac{\Delta p}{q}$$

thus, neglecting terms in $(\Delta x)^2$,

$$B_A R_A + \left(\frac{\partial B}{\partial x}\right)_0 R_A \Delta x + B_A \Delta x = \frac{p_A}{q} + \frac{\Delta p}{q},$$

1027 which, given $B_A R_A = \frac{p_A}{q}$, leaves $\Delta x \left[\left(\frac{\partial B}{\partial x}\right)_A R_A + B_A \right] = \frac{\Delta p}{q}$, which given $k =$

1028 $\frac{R_A}{B_A} \left(\frac{\partial B}{\partial x}\right)_0$ yields

$$\Delta x = \frac{R_A}{1+k} \frac{\Delta p}{p_A} \quad (3.19)$$

1029 Drop the indices, take p as a reference momentum and R as the corresponding
1030 reference orbit radius, this leaves

$$\Delta x = D \frac{\Delta p}{p} \quad \text{with} \quad D = \frac{R}{1+k}, \quad \text{dispersion function} \quad (3.20)$$

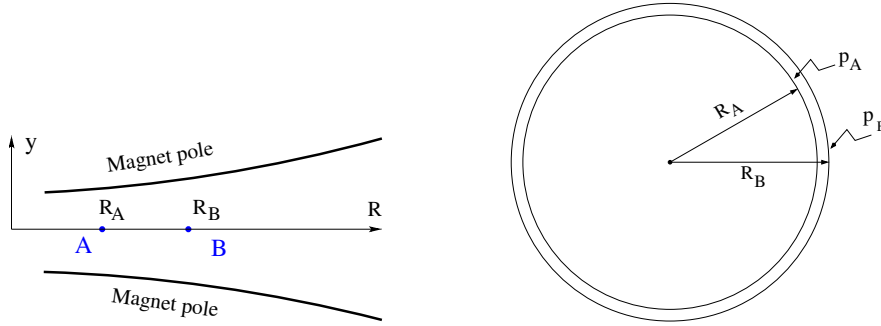


Fig. 3.12 The equilibrium radius at location A is $R = R_A$, the equilibrium momentum is p_A , rigidity $BR = B_A R_A$. The equilibrium radius at B is $R = R_B$, equilibrium momentum p_B , rigidity $BR = B_B R_B$

1031 The dispersion D is an s -independent quantity in the classical cyclotron as a result of
 1032 the cylindrical symmetry of the field (k and $R=p/qB$ are s -independent), and varies
 1033 with R and $k(R)$.

1034 To the first order in the coordinates, the vertical coordinates $y(s)$, $y'(s)$ (Eq. 3.16)
 1035 are unchanged under the effect of a momentum offset, the horizontal trajectory angle
 1036 $x'(s)$ is unchanged as well (the circular orbits are concentric, Fig. 3.12) whereas

$$x(s, p + \Delta p) = x(s, p) + \Delta p \left. \frac{dx}{dp} \right|_{s,p} = x(s) + D \frac{\Delta p}{p} \quad (3.21)$$

1037 with $x(s)$ as in Eq. 3.15.

1038 *Orbit and revolution period lengthening*

1039 Momentum offset results in closed orbit lengthening $\delta C/C = \delta R/R \equiv \delta x/R$, which,
 1040 given Eq. 3.20, can be written under the form

$$\frac{\delta C}{C} = \alpha \frac{\delta p}{p} \quad \text{with} \quad \alpha = \frac{1}{1+k} = \frac{1}{v_R^2} \quad (3.22)$$

1041 with α the ‘‘momentum compaction’’ and $\alpha > 0$, the closed orbit length increases
 1042 with momentum.

1043 The change in revolution period $T_{\text{rev}} = C/\beta c$ with momentum writes

$$\frac{\delta T_{\text{rev}}}{T_{\text{rev}}} = \frac{\delta C}{C} - \frac{\delta \beta}{\beta} = \left(\alpha - \frac{1}{\gamma^2} \right) \frac{\delta p}{p} \quad (3.23)$$

1044 Given that $-1 < k < 0$ and $\gamma \gtrsim 1$, it results that $\alpha - 1/\gamma^2 > 0$ thus $\delta T_{\text{rev}}/T_{\text{rev}} > 0$ as
 1045 expected: the revolution period increases with energy, the increase in radius is faster
 1046 than the velocity increase.

1047 3.1.3 Quasi-Isochronous Resonant Acceleration

1048 An oscillating radio-frequency (RF) electric field, with fixed-frequency f_{rf} is applied
 1049 across the gap between the two dees (Fig. 3.1). An ion of charge q reaching the gap
 1050 at time t undergoes a change in energy

$$\Delta W(t) = q\hat{V} \sin \phi, \quad \text{with} \quad \phi = \omega_{\text{rf}}t - (\omega_{\text{rev}}t + \phi_0) \quad (3.24)$$

1051 with ϕ the RF phase experienced by the particle at the time it crosses the gap and ϕ_0
 1052 the origin in phase for the particle motion. This ignores the “transit time”, the effect
 1053 of the time that the particle spends across the gap on the overall energy gain.

1054 The frequency dependence of the kinetic energy W of the ion relates to its orbital
 1055 radius R in the following way:

$$W = \frac{1}{2}mv^2 = \frac{1}{2}m(2\pi Rf_{\text{rev}})^2 = \frac{1}{2}m(2\pi R\frac{f_{\text{rf}}}{h})^2 \quad (3.25)$$

1056 thus, given cyclotron size (R), f_{rf} and h set the limit for the acceleration range.

1057 The revolution frequency decreases with energy and the condition of synchronism
 1058 with the oscillating voltage, $f_{\text{rf}} = hf_{\text{rev}}$, is only fulfilled at one particular radius in
 1059 the course of acceleration, where $\omega_{\text{rf}} = qB/m$ (Fig. 3.13). Upstream and downstream
 1060 of that radius, out-phasing $\Delta\phi$ builds-up turn after turn, decreasing in a first stage
 1061 (towards lower voltages in Fig. 3.13-right) and then increasing back to $\phi = \pi/2$ and
 beyond towards π . Beyond $\phi = \pi$ the RF voltage is decelerating.

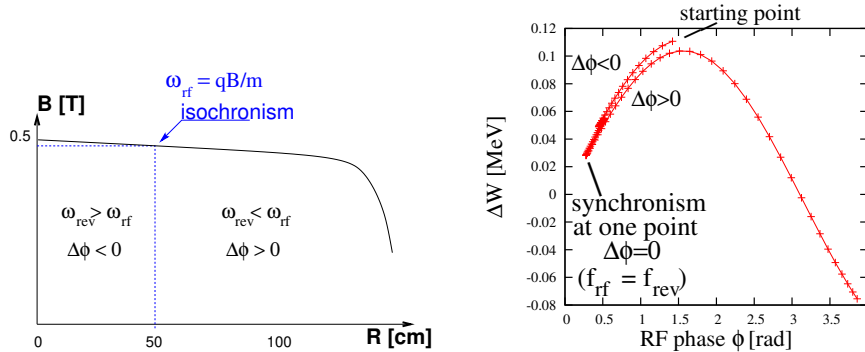


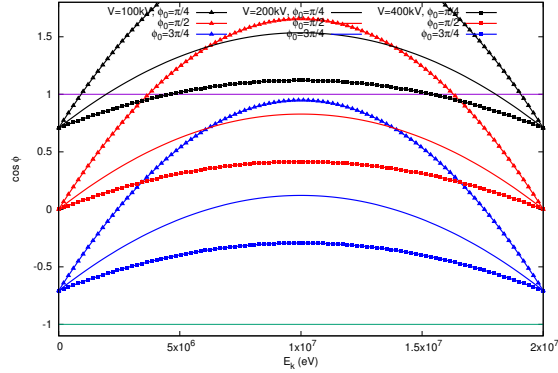
Fig. 3.13 A sketch of the synchronism condition at one point (left, $h=1$ assumed), and the span in phase of the energy gain $\Delta W = q\hat{V} \sin \phi$ over the acceleration cycle (right). ϕ is the phase of the RF sine wave at arrival of the particle at the accelerating gap (the vertical separation of the two $\Delta W(\phi)$ branches on the right ($\Delta\phi < 0$ and $\Delta\phi > 0$) is artificial, this is for clarity, they are actually superimposed)

1062 Differentiating the particle phase at the RF gap (Eq. 3.24), over a half-turn, with
 1063 ω_{rev} constant between two gap passages, one gets $\dot{\phi} = \omega_{\text{rf}} - \omega_{\text{rev}}$. Between two gap
 1064 passages on the other hand, $\Delta\phi = \dot{\phi}\Delta T = \dot{\phi}T_{\text{rev}}/2 = \dot{\phi}\frac{\pi R}{v}$, yielding a phase-shift of
 1065

$$\text{half-turn } \Delta\phi = \pi \left(\frac{\omega_{\text{rf}}}{\omega_{\text{rev}}(R)} - 1 \right) = \pi \left(\frac{m\omega_{\text{rf}}}{qB(R)} - 1 \right) \quad (3.26)$$

1066 The out-phasing is thus a gap-after-gap, cumulative effect. Due to this the classical
 1067 cyclotron requires quick acceleration (limited number of turns), which means
 1068 high voltage (tens to hundreds of kVolts). As expected, with ω_{rf} and B constant, ϕ
 1069 presents a minimum ($\dot{\phi} = 0$) at $\omega_{\text{rf}} = \omega_{\text{rev}} = \frac{qB}{m}$ where exact isochronism is reached
 1070 (Fig. 3.13). The upper limit to ϕ is set by the condition $\Delta W > 0$: acceleration.

Fig. 3.14 A graph of the cyclotron equation (Eq. 3.27), for a few different RF settings. The sole settings resulting in a $\cos \phi$ curve comprised in $[-1, 1]$ allow complete acceleration from injection to top energy. For instance, for injection $\phi_0 = \pi/4$, acceleration to 20 MeV is not possible (upper three curves). Acceleration to 20 MeV works with $\phi_0 = 3\pi/4$, with as low as 100 kV/gap (lower three curves)



1071 The cyclotron equation determines the achievable energy range, depending on
 1072 the injection energy E_0 , the RF phase at injection ϕ_0 , the RF frequency ω_{rf} and gap
 1073 voltage \hat{V} , following [12]

$$\cos \phi = \cos \phi_0 + \pi \left[1 - \frac{\omega_{\text{rf}}}{\omega_{\text{rev}}} \frac{E + E_0}{2M} \right] \frac{E - E_0}{q\hat{V}} \quad (3.27)$$

1074 ($E = E_k + M$ is the total energy, M is the rest mass, the index 0 denotes injection
 1075 parameters) and is represented in Fig. 3.14 for various values of the RF voltage and
 1076 phase at injection ϕ_0 .

1077 3.1.4 Extraction

1078 From $R = p/qB$ and assuming constant field (legitimate in the presence of a very
 1079 small field index), with kinetic energy $E_k = p^2/2M$ in the non-relativistic approxi-
 1080 mation ($E_k \ll M$), one gets

$$\frac{dR}{R} = \frac{1}{2} \frac{dE_k}{E_k} \quad (3.28)$$

1081 Integrating the right hand side equality yields

$$R^2 = R_0^2 \frac{E_k}{E_{k,0}} \quad (3.29)$$

1082 with R_0 , $E_{k,0}$ initial conditions. From Eqs. 3.28, 3.29, assuming $E_{k,0} \ll E_k$ and
 1083 constant acceleration rate dE_k such that $E_k = n dE_k$ after n turns, one gets the
 1084 scaling laws

$$R \propto \sqrt{n}, \quad dR \propto \frac{R}{E_k} \propto \frac{1}{R} \propto dE_k, \quad \frac{dR}{dn} = \frac{R}{2n} \quad (3.30)$$

1085 so that, in particular, the turn separation dR/dn is proportional to the average orbit
 1086 radius R and to the energy gain per turn.

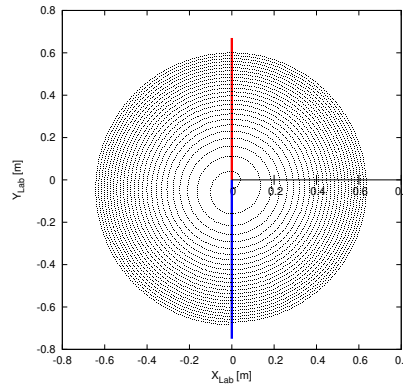


Fig. 3.15 The radial distance between successive turns decreases with energy, in inverse proportion to the orbit radius

1087 The radial distance between successive turns decreases with energy, toward zero
 1088 (Fig. 3.15), eventually resulting in insufficient spacing for insertion of an extraction
 1089 septum.

1090 *Betatron modulation*

1091 Consider a particle bunch injected in the cyclotron with some (x_0, x'_0) conditions, and
 1092 assume very slow acceleration. While accelerated the bunch undergoes a betatron
 1093 motion around the local closed orbit, following Eq. 3.15. Observed at some azimuth
 1094 s , this betatron oscillation modulates the distance of the bunch to the local reference
 1095 closed orbit, moving it outward or inward depending on the turn number, which
 1096 means a modulation of the distance between the accelerated turns: an effect that
 1097 can be exploited for increasing the separation of consecutive orbits at extraction to
 1098 enhance the extraction efficiency [8].

1099 3.1.5 Spin Dance

1100 An effect of a magnetic field \mathbf{B} on a spin angular momentum \mathbf{S} , as a consequence of
1101 the resulting torque, is the spin precession, around the precession vector (Sec. 18.6.1)

$$\omega_{\text{sp}} = \frac{q}{m} [\mathbf{B} + G(\mathbf{B}_{\parallel} + \gamma\mathbf{B}_{\perp})] \quad (3.31)$$

1102 at an angular frequency $|\omega_{\text{sp}}|$, with $\mathbf{B} = \mathbf{B}_{\parallel} + \mathbf{B}_{\perp}$, \mathbf{B}_{\parallel} and \mathbf{B}_{\perp} the magnetic field
1103 components respectively parallel and normal to the particle velocity, and G the
1104 anomalous gyromagnetic factor:

1105 $G=1.7928474$ (proton), -0.178 (Li), -0.143 (deuteron), -4.184 (^3He) ...

1106 The spin precession in \mathbf{B} satisfies the Thomas-BMT differential equation

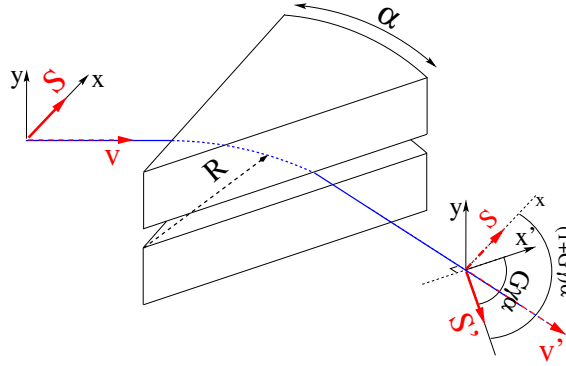
$$\frac{d\mathbf{S}}{dt} = \mathbf{S} \times \omega_{\text{sp}} \quad (3.32)$$

1107 If the particle moves in the median plane of a cyclotron then $\mathbf{B}_{\parallel} = 0$ and the
1108 precession axis is parallel to the magnetic field vector, \mathbf{B}_y , namely $\omega_{\text{sp}} = \frac{q}{m} (1 +$
1109 $G\gamma)\mathbf{B}_y$. The precession angle writes

$$\theta_{\text{sp, Lab}} = \frac{1}{v} \int \omega_{\text{sp}} ds = (1 + G\gamma) \frac{\int B ds}{BR} = (1 + G\gamma)\alpha \quad (3.33)$$

with α the trajectory bend angle (Fig. 3.16). The precession angle in the moving

Fig. 3.16 Spin and velocity vector precession in a constant field, from \mathbf{S} to \mathbf{S}' and \mathbf{v} to \mathbf{v}' respectively. In the moving frame the spin precession along the arc $\mathcal{L} = R\alpha$ is $G\gamma\alpha$, in the laboratory frame the spin precesses by $(1 + G\gamma)\alpha$



1110 frame (the latter rotates by an angle α across the magnet) is

$$\theta_{\text{sp}} = G\gamma\alpha \quad (3.34)$$

1112 from what it results that the number of precessions per turn is $G\gamma$. By analogy with
1113 the betatron tune (the number of sinusoidal oscillations per turn around the reference
1114 circle, Eq. 3.17) this defines the spin tune

$$\nu_{\text{sp}} = G\gamma$$

(3.35)

1115 3.2 Exercises

1116 Preliminaries

- 1117 • Zgoubi users' guide at hand, when setting up the input data files to work out
 1118 the exercises, is a must-have. PART B of the guide in particular, details the
 1119 formatting of the input data lists following keywords (a few keywords only, for
 1120 instance FAISCEAU, MARKER, YMY, do not require additional data), and gives
 1121 the units to be used.
- 1122 • About keywords: by "keyword" it is meant, the name of the optical elements,
 1123 or I/O procedures, or commands, as they appear in simulation input data file.
 1124 Keywords are most of the time referred to without any additional explanation: it
 1125 is understood that the users' guide is at hand, and details regarding the use and
 1126 functioning to be sought there: in PART A of the guide, as to what a particular
 1127 keyword does and how it does it; in PART B as to the formatting of the data
 1128 list under a particular keyword. The users' guide INDEX is a convenient tool to
 1129 navigate through the keywords.
- 1130 – The notation KEYWORDS[ARGUMENT1, ARGUMENT2, ...]: it uses the
 1131 nomenclature found in the Users' Guide, Part B. Consider a couple of exam-
 1132 ples:
 1133 · OBJET[KOBJ=1] stands for keyword OBJET, and the value of KOBJ=1
 1134 retained here;
 1135 · OPTIONS[CONSTY=ON] stands for keyword OPTIONS, and the option
 1136 retained here, CONSTY, switched ON.
- 1137 – The keyword INCLUDE is used in many simulation input data files. The reason
 1138 is mostly to reduce the length of these files. It may always be replaced by the
 1139 sequence that it INCLUDEs.
- Coordinate Systems: two sets of coordinate notations are used in the exercises,

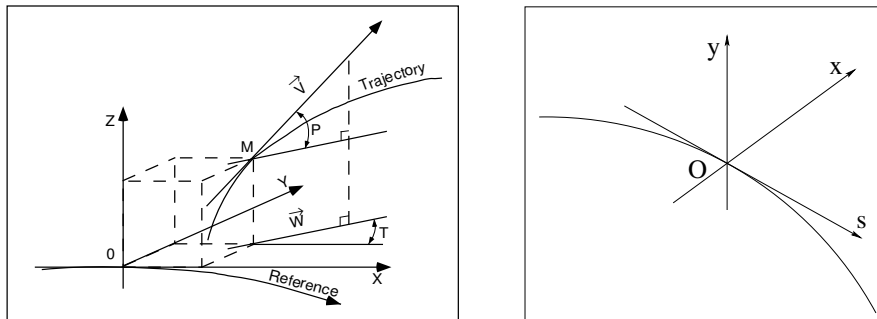


Fig. 3.17 Zgoubi Cartesian frame (O;X,Y,Z), and moving frame (O;s,x,y)

- 1141 – on the one hand (and, in the Solutions Section mostly), zgoubi's (Y,T,Z,P,X,D)
 1142 coordinates in the optical element reference frame (O;X,Y,Z), the very frame
 1143 in which the optical element field $\mathbf{E}(X, Y, Z)$ and/or $\mathbf{B}(X, Y, Z)$ is defined (the
 1144 origin for X depends on the optical element). Particle coordinates in this frame
 1145 can be
- 1146 · either Cartesian, in which case X, Y (angle T) and Z (angle P) denote
 - 1147 respectively the longitudinal, transverse horizontal and vertical coordinates,
 - 1148 · or cylindrical, in which case, given m the projection of particle position M
 - 1149 in the $Z=0$ plane, Y denotes the radius: $Y = |\mathbf{Om}|$, whereas X denotes the
 - 1150 **OX-Om** angle (and, yes, the nature of the variables named X and Y in the
 - 1151 source code does change);

Note: the sixth zgoubi's coordinate above is

$$D = \frac{\text{particle rigidity}}{BORO}$$

1152 with BORO a reference rigidity, the very first numerical datum to appear in
 1153 any zgoubi sequence, as part of the definition of initial particle coordinates by
 1154 OBJET or MCOBJET. BORO may sometimes be denoted $B\rho_{\text{ref}}$, depending
 1155 upon the context. Note that D-1 identifies with the above $\delta p/p$.

- 1156 – on the other hand (and, in the exercise assignments mostly), the conventional
 1157 $(x, x', y, y', \delta l, \delta p/p)$ coordinates in the moving frame (O;s,x,y) or close variants.

1158 Comments are introduced wherever deemed necessary (hopefully, often enough)
 1159 in an effort to lift potential ambiguities regarding coordinate notations.

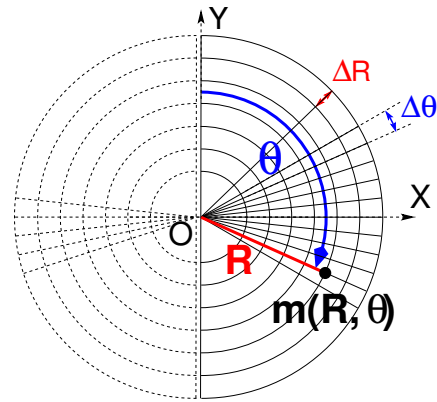
1160 3.1 Modeling a Cyclotron Dipole: Field Map

1161 In this exercise, a cyclotron dipole field is simulated using a field map. A field
 1162 map is an easy way to simulate a magnet, this is a major interest of the method. It can
 1163 account for fancy geometries and fields, including field index and non-linearities,
 1164 field defects. Depending on field symmetries it may be 1-, 2-, or 3-dimensional. It can
 1165 be generated using mathematical field models, or from magnet computation codes, or
 1166 from magnetic measurements. In this exercise a model of a cyclotron field is devised
 1167 using such field map method. The model is based on a calculated two-dimensional
 1168 map of the mid-plane field, with 180 deg or 60 deg angular extent; TOSCA keyword
 1169 is used to raytrace through these maps.

1170 The first step in this exercise consists in fabricating that field map.

1171 A 2-dimensional $m(R, \theta)$ polar meshing of the median plane is considered
 1172 (Fig. 3.18). It is defined in a (O; X, Y) frame and covers a 180° sector (or 60 deg, in
 1173 some of the exercises). The median plane field map provides the values of the field
 1174 components $B_Z(R, \theta)$ normal to the $Z = 0$ plane, at the nodes of the mesh. Note
 1175 that a single 360° field map could be used instead, however implementing two 180°
 1176 sectors will allow further insertion of an accelerating gap, between the two 180°
 1177 sectors. Computation of the field along (R, θ) particle trajectories in the (O;X,Y,Z)
 1178 frame is performed from the field map data, using interpolation techniques [13].

Fig. 3.18 Principle of a field map in a polar coordinate system, covering a 180° sector (over the right hand side dee). The mesh nodes $m(R, \theta)$ are distant ΔR radially, $\Delta\theta$ azimuthally. The map is used twice, so covering the 360° cyclotron dipole as sketched here, while allowing further insertion of an accelerating gap between the two dees



1179 (a) Construct a 180° two-dimensional map of a median plane field $B_Z(R, \theta)$,
 1180 proper to simulate the field in a cyclotron as sketched in Fig. 3.1. Use a uniform
 1181 mesh in a polar coordinate system (R, θ) as sketched in Fig. 3.18, covering from $R=1$
 1182 to 76 cm. Take a radial increment of the mesh $\Delta R = 0.5$ cm, azimuthal increment
 1183 $\Delta\theta = 0.5$ cm/RM, RM some arbitrary reference radius (say, 50 cm, here), and
 1184 constant axial field $B_Z = 0.5$ T. The appropriate 6-column formatting of the field
 1185 map data for TOSCA to read them is the following:

$$R \cos \theta, Z, R \sin \theta, B_Y, B_Z, B_X$$

1186
 1187 with θ varying first, R varying second in that list. Z is the vertical direction (normal
 1188 to the map mesh), $Z \equiv 0$.

1189 Plot $B_Z(R, \theta)$.

1190 (b) Raytrace a few concentric circular mid-plane trajectories centered on the
 1191 center of the dipole, ranging in $10 \leq R \leq 80$ cm. Plot these concentric trajectories
 1192 in the $(O; X, Y)$ laboratory frame. Initial coordinates can be defined using OBJET,
 1193 particle coordinates along trajectories during the stepwise raytracing can be logged
 1194 in zgoubi.plt by setting IL=2 under TOSCA.

1195 Explain why it is possible to push the raytracing beyond the 76 cm radius field
 1196 map extent, without loss of accuracy.

1197 (c) Compute the orbit radius R and the revolution period T_{rev} as a function of
 1198 kinetic energy E_k , or rigidity BR . Produce a graph, including for comparison the
 1199 theoretical dependence of T_{rev} . Explain what causes the slow increase of revolution
 1200 period with energy.

1201 (d) Check the effect of the density of the mesh (the choice of ΔR and $\Delta\theta$ values,
 1202 *i.e.*, the number of nodes $N_\theta \times N_R = (1 + \frac{180^\circ}{\Delta\theta}) \times (1 + \frac{80 \text{ cm}}{\Delta R})$), on the accuracy of the
 1203 trajectory and time-of-flight computation.

1204 (e) Consider a mesh with such ΔR , $\Delta\theta$ density as to ensure reasonably good
 1205 convergence of the numerical resolution of the differential equation of motion [13,
 1206 Eq. 1.2.4].

1207 Check the effect of the integration step size on the accuracy of the trajectory
 1208 and time-of-flight computation, by considering a small $\Delta s = 1$ cm and a large
 1209 $\Delta s = 20$ cm, at 200 keV and 5 MeV (assume proton).

1210 (f) Consider a periodic orbit, thus its radius R should remain unchanged after
 1211 stepwise integration of the motion over a turn. However, the size Δs of the numerical
 1212 integration step has an effect on the final value of the radius:

1213 for two different cases, 200 keV (a small orbit) and 5 MeV (a larger one), provide
 1214 the dependence of the relative error $\delta R/R$ after one turn, on the integration step size
 1215 Δs (consider a series of Δs values in a range $\Delta s : 0.1 \text{ mm} \rightarrow 20 \text{ cm}$). Plot the two
 1216 $\frac{\delta R}{R}(\Delta s)$ curves (200 keV and 5 MeV), explain their upward concavity.

1217 3.2 Modeling a Cyclotron Dipole: Analytical

1218 In this exercise the vector field $\mathbf{B}(R, \theta, Z)$ at the location (R, θ, Z) of the parti-
 1219 cle along its trajectory is determined using an analytical modeling (as opposed to
 1220 interpolating from a field map as in exercise 3.1).

1221 Use DIPOLE for instance among other possible choices. DIPOLE provides an
 1222 analytical modeling of the median plane field $\mathbf{B}(R, \theta, Z = 0)$, and extrapolation off
 1223 the median plane uses Taylor expansions accounting for Maxwell's equations.

1224 (a) Repeat questions (b), (c) and (e) of exercise 3.1.

1225 (b) From the two series of results (exercises 3.1 and the present one), comment on
 1226 various pros and cons of the two methods, field map versus analytical field model.

1227 3.3 Geometrical Focusing

1228 Because the field is constant over the all space ($\mathbf{B} \equiv \mathbf{B}_Z$ and $|\mathbf{B}_Z| = \text{constant}$, \forall
 1229 X, Y, Z), there is no vertical focusing: any trajectory with a non-zero vertical angle
 1230 would spiral away, vertically.

1231 (a) Using the foregoing field model, verify that this is what the numerical inte-
 1232 gration yields.

1233 Produce a 3-D plot of the trajectory, superpose theory (give the parametric equa-
 1234 tions of motion) and numerical integration.

1235 (b) Instead, horizontal motion features geometrical focusing, this is due to the
 1236 trajectory curvature. Show the geometrical focusing graphically.

1237 3.4 Relativistic Kinematic Relationships

1238 In the subsequent exercises, relativistic kinematic quantities will be used, this
 1239 exercises introduces some differential relations between them which will also be
 1240 resorted to.

1241 (a) Demonstrate the following relativistic relations (M =rest mass, E_k =kinetic
 1242 energy, $E = E_k + M$, $c=1$; γ may vary in electrostatic elements or in the RF cavities
 1243 of an accelerator):

$$\begin{aligned}
 1244 \quad \frac{dp}{p} &= \frac{1}{\beta^2} \frac{dE}{E}, & dp &= \frac{dE}{\beta} \\
 1245 \quad \frac{dv}{v} &= \frac{d\beta}{\beta} = \frac{1}{\gamma^2} \frac{dp}{p} = \frac{1}{\beta^2 \gamma^2} \frac{dE}{E} = \frac{1}{\beta^2 \gamma^2} \frac{d\gamma}{\gamma} \\
 1246 \quad \frac{d\gamma}{\gamma} &= \frac{dE}{E} = \frac{dM\gamma}{M\gamma} = \frac{dE_k}{E_k + M} \\
 1247 \quad \frac{dE}{E - M} &= \frac{dE_k}{E_k} = \frac{\gamma + 1}{\gamma} \frac{dp}{p}
 \end{aligned}$$

1248 (b) Produce the evolution of these quantities numerically, compare these numerical
1249 results with theoretical expectations from (a).

1250 (c) Using the random particle generator MCOBJET, produce a 2×10^4 bunch
1251 of protons with Gaussian dp/p , $\sigma_{dp/p} = 10^{-3}$. Plot some of the densities above and
1252 check the equalities in (a).

1253 3.5 Resonant Acceleration

1254 Based on the earlier dipole sector, using indifferently a field map or an analytical
1255 model of the field, introduce an accelerating gap between the two dees with peak
1256 voltage 100 kV. Assume that particle motion does not depend on RF phase: the boost
1257 through the gap is the same at all passes, CAVITE[IOPT=3] can be used for that.

1258 (a) Accelerate a proton with initial kinetic energy 20 keV, up to 5 MeV, take
1259 harmonic $h=1$. Plot the accelerated trajectory in a (O; X, Y) frame similar to that in
1260 Fig. 3.18.

1261 (b) Plot the proton momentum p and total energy E as a function of its kinetic
1262 energy, both from this numerical experiment (raytracing data can be stored using
1263 FAISTORE) and from theory, everything on the same graph.

1264 (c) Plot the normalized velocity $\beta = v/c$ as a function of kinetic energy, both
1265 numerical and theoretical, and in the latter case both classical and relativistic.

1266 (d) Plot the relative change in velocity $\Delta\beta/\beta$ and the relative change in circum-
1267 ference $\Delta C/C$, as a function of kinetic energy. both numerical and theoretical. From
1268 their evolution, conclude that the time of flight increases with energy.

1269 3.6 Resonant Acceleration (2)

1270 Re-do the previous exercise, assuming a harmonic $h=3$ RF frequency.

1271 3.7 Visit High Energies

1272 Forget the fact that this not possible in a classical cyclotron (use CAVITE[IOPT=3]),
1273 and push proton energy to 3 GeV kinetic, re-do questions (a) to (d) of Ex. 3.5.

1274 Note:

1275 - pushing the energy in this manner is only possible if acceleration at the gap is
1276 independent of particle phase, hence the necessary choice of CAVITE[IOPT=3],

1277 - if a field map model is used, it is perhaps, or perhaps not, necessary to extend the
1278 radial extent of the mesh to encompass the spiraling trajectory up to 3 GeV - please
1279 clarify that point,

1280 - in the case the analytical model DIPOLE is used instead, surely no modification
1281 is needed, its data remain unchanged, figure that out.

1282 3.8 Spin Dance

1283 (a) From the analogy between the vector precession equations,

$$1284 \quad \dot{\mathbf{v}} = \frac{q}{m} \mathbf{v} \times \mathbf{B}, \quad \text{particle velocity vector, on the one hand}$$

$$1285 \quad \dot{\mathbf{S}} = \mathbf{S} \times \boldsymbol{\omega}_{\text{sp}}, \quad \text{particle spin vector, on the other hand (Eq. 18.28),}$$

1286 and from the expression for the particle trajectory rotation angle $\alpha = \int B ds / BR$ as
1287 stems from the former, deduce the expression for the spin rotation angle in constant
1288 vertical B field - no calculations needed.

1289 In the following the cyclotron model of exercise 3.1 or 3.2 indifferently can be
1290 used.

1291 (b) Add spin transport, using SPNTRK. Produce a listing (zgoubi.res) of a simu-
1292 lation, including spin outcomes.

1293 Note: PARTICUL is necessary here, in order for the equation of motion to be
1294 solved [13, Sec. 2]. SPNPRT can be used to have local spin coordinates listed in
1295 zgoubi.res (at the manner FAISCEAU lists particle coordinates).

1296 (c) Consider proton case, initial spin longitudinal, compute the spin precession
1297 over one revolution, as a function of energy over a range 12 keV→5 MeV. Give a
1298 graphical comparison with theory.

1299 FAISTORE can be used to store local particle data, which include spin coordi-
1300 nates, in a zgoubi.fai style output file. IL=2 can be used to obtain a print out of
1301 particle motion data to zgoubi.plt during stepwise integration.

1302 (d) Inject a proton with longitudinal initial spin S_z . Give a graphic of the longi-
1303 tudinal spin component motion as a function of azimuthal angle, over a few turns
1304 around the ring. Deduce the spin tune from this computation. Repeat for a couple of
1305 different energies.

1306 Place both FAISCEAU and SPNPRT commands right after the first dipole sector,
1307 and use them to check the spin rotation and its relationship to particle rotation, right
1308 after the first passage through that first sector.

1309 (e) Spin dance: the optical sequence here is assumed to be a complete turn (*i.e.*,
1310 six DIPOLES if a 60 deg DIPOLE model is used). Inject an initial spin at an angle
1311 from the horizontal plane (this is in order to have a non-zero vertical component),
1312 produce a 3-D animation of the spin dance around the ring, over a few turns.

1313 (f) Repeat questions (b-e) for two additional particles: deuteron (much slower
1314 spin precession), $^3\text{He}^{2+}$ (much faster spin precession).

1315 3.9 Synchronized Spin Torque

1316 A synchronized spin kick is superimposed on orbital motion. A input data file
1317 accounting the simulation of a complete cyclotron is considered as in (e), for
1318 instance six 60 degree DIPOLES, or two 180 degree DIPOLES, etc.

1319 Insert a spin rotation of a few degrees around the longitudinal axis, at the end
1320 of the optical sequence (*i.e.*, after one orbit around the cyclotron). SPINR can be
1321 used for that, to avoid any orbital effect. Track 4 particles on their closed orbit, with
1322 respective energies 0.2, 108.412, 118.878 and 160.746 MeV.

1323 Produce a graph of the motion of the vertical spin component S_y along the circular
1324 orbit.

1325 Produce a graph of the spin vector motion on a sphere.

1326 Explain the results.

1327 3.10 Introducing a Radial Field Index

1328 (a) Reproduce Fig. 3.10.

1329 (b) Ray trace over a few turns with some $-1 < k < 0$ value, to show the sinusoidal
1330 horizontal motion. Show the horizontal motion instability when $k < -1$.

1331 (c) Add vertical motion and show the vertical sinusoidal oscillation with $k < 0$,
1332 show the vertical instability if $k > 0$.

1333 3.11 Weak Focusing

1334 (a) Consider a 60° sector as in earlier exercises (building a field map as in
 1335 exercise 3.1, or using DIPOLE as in exercise 3.2), construct the sector accounting
 1336 for a non-zero radial index k in order to introduce vertical focusing, say $k = -0.03$,
 1337 assume a reference radius R_0 for a reference energy of 200 keV (R_0 and B_0 are
 1338 required in order to define the index k , Eq. 3.12). Raytrace that 200 keV reference
 1339 orbit, plot it in the lab frame: make sure it comes out as expected, namely, constant
 1340 radius, final and initial angles equal (normally null given the working hypotheses, as
 1341 established in previous exercises).

1342 (b) Find and plot the radius dependence of orbit rigidity, $BR(R)$, from raytracing
 1343 over a BR range covering 20 keV to 5 MeV.

1344 (c) Plot the axial paraxial motion of a 1 MeV proton, over a few turns (use $IL=2$
 1345 under TOSCA to have stepwise integration data logged in `zgoubi.plt`). Check the
 1346 effect of the focusing strength by comparing the trajectories for a few different index
 1347 values, including close to -1 and close to 0 .

1348 (d) Plot the magnetic field experienced by the particle along these trajectories.

1349 3.12 Loss of Isochronism

1350 Compare on a common graphic the revolution period $T_{\text{rev}}(R)$ for a field index
 1351 value $k \approx -0.95, -0.5, -0.03, 0^-$. The scan method of exercise 3.11, based on
 1352 REBELOTE, can be referred to.

1353 3.13 Particle Trajectories

1354 In this exercise individual particle trajectories are computed. DIPOLE or TOSCA
 1355 can be used, indifferently. No acceleration in this exercise, particles cycle around the
 1356 cyclotron at constant energy.

1357 (a) Plot the horizontal and vertical trajectory components $x(s)$ and $y(s)$ of a particle
 1358 with rigidity close to $BR(R_0)$ (R_0 is the reference radius in the definition of the index
 1359 k), over a few turns around the cyclotron. From the number of turns, give an estimate
 1360 of the wave numbers. Check the agreement with the expected $\nu_R(k)$, $\nu_Y(k)$ values
 1361 from Eq. 3.17.

1362 Consider particle energies of 1 MeV and 5 MeV, far from the reference kinetic
 1363 energy $E(R_0)$; the wave numbers change with energy: could that be expected? Find
 1364 their theoretical values, compare with numerical outcomes.

1365 (b) In the former case, 200 keV energy, plot as a function of s the difference
 1366 between $x(s)$ from raytracing and its values from Eq. 3.15. Same for $y(s)$ compared
 1367 to Eq. 3.16. Is there agreement? (use the option $IL=2$ to store particle coordinates in
 1368 `zgoubi.plt`, step-by-step).

1369 3.14 Energy Dependence of Wave Numbers

1370 Perform a scan of the wave numbers over 200 keV–5 MeV energy interval, com-
 1371 puted using MATRIX, and using REBELOTE to repeat MATRIX computation for
 1372 a series of energy values.

1373 3.15 Phase Space Motion, Fourier Analysis

1374 This exercise introduces to phase space and phase space motion, and to spectral
 1375 analysis of particle motion.

1376 Raytrace a particle with small amplitude radial and axial oscillations with respect
1377 to the reference circular closed orbit (paraxial motion), at constant energy.

1378 (a) At some fixed azimuth s around the cyclotron, observe the radial excursion
1379 $(x(n), x'(n))$ of the particle as it cycles around for many turns (n is the turn number)
1380 (use FAISTORE to store particle coordinates in `zgoubi.fai`, turn by turn). Plot
1381 $(x(n), x'(n))$ in the transverse phase-space (x, x') .

1382 Repeat for (y, y') .

1383 (b) From the trajectory equation (Eq. 3.15, radial motion, or Eq. 3.16, axial
1384 motion), show that particle motion in phase space is on an ellipse. Calculate the
1385 ellipse parameters. Verify graphically that it superposes on the particle motion from
1386 multiturn raytracing.

1387 (c) Compute the radial and axial wave numbers by Fourier analysis of respectively
1388 the $x(n)$ and the $y(n)$ motion. Check the agreement with the expected $\nu_R(k)$, $\nu_y(k)$
1389 values from theory.

1390 (d) Constant energy motion spectrum:

1391 (i) there is an indetermination on the value of the wave number, from the Fourier
1392 analysis, explain

1393 (ii) give a theoretical calculation of the accuracy on the position of the peak from
1394 the DFT technique. Check this against the numerical computation by varying the
1395 spectrum sampling in the DFT series

1396 (iii) explain the origin of the $\sin u/u$ shape of the spectrum. Calculate the spacing
1397 between the zeroes, from theory, compare with the zeroes of the numerical DFT.

1398 3.16 RF Phase at the Accelerating Gap

1399 (a) Consider the cyclotron model of exercise 3.11: two dees, double accelerating
1400 gap, field index $k = -0.03$ defined at $R_0 = 50$ cm, field $B_0 = 5$ kG on that radius.

Raytrace a proton trajectory from 1 to 5 MeV: get the turn-by-turn phase-shift at
the gaps, compare with (Eq. 3.26)

$$\text{half-turn } \Delta\phi = \pi \left(\frac{\omega_{\text{rf}}}{\omega_{\text{rev}}(R)} - 1 \right) = \pi \left(\frac{m\omega_{\text{rf}}}{qB(R)} - 1 \right)$$

1401 Produce a similar diagram $\Delta W(\phi)$ to Fig. 3.13-right.

1402 Accelerate over more turns, observe the particle decelerate.

1403 (b) Repeat (a) for the index definition of exercise 3.11: $k=-0.03$, defined on the
1404 200 keV injection radius $R_0 = 12.924888$ cm, with $B_0 = 5$ kG.

1405 3.17 The Cyclotron Equation

1406 Cyclotron model settings of exercise 3.5 are first considered in questions (a) to (c):
1407 two dees, double accelerating gap, uniform field $B = 0.5$ T (a field map or analytical
1408 field modeling can be used, indifferently). In question (d) a field index is introduced.

1409 (a) Set up an input data file for the simulation of a proton acceleration from
1410 0.2 to 20 MeV. In particular, assume that $\cos(\phi)$ reaches its maximum value at
1411 $W_m = 10$ MeV; find the RF voltage frequency from $d(\cos \phi)/dW = 0$ at W_m .

(b) Give a graph of the energy-phase relationship (Eq. 3.27)

$$\cos \phi = \cos \phi_0 + \pi \left[1 - \frac{\omega_{rf}}{\omega_{rev}} \frac{E + E_0}{2M} \right] \frac{E - E_0}{q\hat{V}}$$

1412 for $\phi_0 = \frac{3\pi}{4}, \frac{\pi}{2}, \frac{\pi}{4}$, from both simulation and theory.

1413 (c) Re-do the exercise using an RF frequency third harmonic of the revolution
1414 frequency, in the same double-dee configuration.

1415 (d) Repeat (a) and (b) for the index definition of exercise 3.11: $k=-0.03$, defined
1416 on the 200 keV injection radius $R_0 = 12.924888$ cm, with $B_0 = 5$ kG.

1417 3.18 Cyclotron Extraction

1418 (a) Acceleration of a proton in a uniform field $B=0.5$ T is first considered, this is
1419 the case of exercise 3.5.

1420 Compute the distance ΔR between turns, as a function of turn number and of
1421 energy, over the range $E : 0.02 \rightarrow 5$ MeV. Compare graphically with theoretical
1422 expectation.

1423 (b) Assume a beam with Gaussian momentum distribution and *rms* momentum
1424 spread $\delta p/p = 10^{-3}$. An extraction septum is placed half-way between two successive
1425 turns, plot the percentage of beam loss at extraction, as a function of extraction turn
1426 number - COLLIMA can be used for that simulation and for particle counts, it also
1427 allows for possible septum thickness.

1428 (c) Repeat (a) and (b) considering a field with index - conditions of exercise 3.10
1429 for instance, $B_0 = 0.5$ T and $k = -0.03$ at $R_0 = R(0.2 \text{ MeV}) = 12.924888$ cm.

1430 (d) Investigate the effect of injection conditions (x_0, x'_0) on the modulation of the
1431 distance between turns.

1432 Show that, with slow acceleration, the oscillation is minimized for an initial
1433 $|x'_0| = \left| \frac{x_0 v_R}{R} \right|$ [8, p. 133].

1434 3.19 Acceleration and Extraction of a 6-D Polarized Bunch

1435 The cyclotron simulation hypotheses of exercise 3.17-a are considered.

1436 Add a short “high energy” line, say 1 meter, for beam extraction downstream of
1437 the cyclotron (which means following REBELOTE in the optical sequence), ending
1438 up with a “Beam_Dump” MARKER.

1439 (a) Create a 1,000 particle bunch with the following initial parameters:

1440 - random Gaussian transverse phase space densities, centered on the closed orbit,
1441 truncated at 3 sigma, normalized *rms* emittances $\epsilon_Y = \epsilon_Z = 1 \pi \mu\text{m}$, both emittances
1442 matched to the 0.2 MeV orbit optics,

1443 - uniform bunch momentum density $0.2 \times (1 - 10^{-3}) \leq p \leq 0.2 \times (1 + 10^{-3})$ MeV,
1444 matched to the dispersion, namely (Eq. 3.21), $\Delta x = D \frac{\Delta p}{p}$,

1445 - random uniform longitudinal distribution $-0.5 \leq s \leq 0.5$ mm,

1446 Note: there is two possibilities to create this object, namely, using either
1447 (i) MCOBJET, or (ii) OBJET[KOBJ=3] which reads an external file containing
1448 particle coordinates.

1449 Add spin tracking request (SPNTRK), all initial spins normal to the bend plane.

1450 Plot the three initial 2-D phase spaces: (Y,T), (Z,P), $(\delta l, \delta p/p)$, check the matching
1451 to the 200 keV optics.

- 1452 Plot the Y, Z, dp/p , δl and S_Z histograms. Check the distribution parameters.
- 1453 (b) Accelerate this polarized bunch to 20 MeV, using the following RF conditions:
- 1454 - 200 kV peak voltage,
- 1455 - RF harmonic 1,
- 1456 - initial RF phase $\phi_0 = \pi/4$.
- 1457 Plot the three phase spaces as observed downstream of the extraction line. Plot
- 1458 the Y, Z, dp/p , δl and S_Z histograms. Compare the distribution parameters with the
- 1459 initial values.
- 1460 What causes the spins to spread away from vertical?

References

- 1461
- 1462 1. Jones, L., Mills, F., Sessler, A., et al.: Innovation Was Not Enough. World Scientific (2010)
- 1463 2. Lawrence, E.O., Livingston, M.S., Phys. Rev. 37, 1707 (1931), 1707; Phys. Rev. 38, 136,
- 1464 (1931); Phys. Rev. 40, 19 (1932)
- 1465 3. Ernest O. Lawrence and M. Stanley Livingston, The Production of High Speed Light Ions
- 1466 Without the Use of High Voltages, Phys. Rev. 40, 19-35 (1932)
- 1467 4. Livingston, M.S., McMillan, Edwin M.: History of the cyclotron. Physics Today, 12(10)
- 1468 (1959).
- 1469 <https://escholarship.org/uc/item/29c6p35w>
- 1470 5. Bethe, H. E., Rose, M. E.: Maximum energy obtainable from cyclotron. Phys. Rev. 52 (1937)
- 1471 1254
- 1472 6. Cole, F.T.: O Camelot ! A memoir of the MURA years (April 1, 1994).
- 1473 <https://accelconf.web.cern.ch/c01/cyc2001/extra/Cole.pdf>
- 1474 7. 4.a L.H.Thomas, *The Paths of Ions in the Cyclotron*, Phys. Rev. 54, 580, (1938)
- 1475 4.b M.K. Craddock, *AG focusing in the Thomas cyclotron of 1938* , Proceedings of PAC09,
- 1476 Vancouver, BC, Canada, FR5REP1
- 1477 8. Stambach, T.: Introduction to Cyclotrons. CERN accelerator school, cyclotrons, linacs and
- 1478 their applications. IBM International Education Centre, La Hulpe, Belgium, 28 April-5 May
- 1479 1994.
- 1480 9. Baron, E., et al.: The GANIL Injector. Proceedings of the 7th International Conference on
- 1481 Cyclotrons and their Applications, ZÄijrich, Switzerland (1975).
- 1482 <http://accelconf.web.cern.ch/c75/papers/b-05.pdf>
- 1483 10. Li, C.Y., et al.: A Permanent Magnet System for a Cyclotron used as a mass spectrometer.
- 1484 11. Lawrence, E.O., Edlefsen, N.E.: On the production of high speed protons. Science, 72, 376-377
- 1485 (1930)
- 1486 12. Le Duff, J.: Longitudinal beam dynamics in circular accelerators. CERN Accelerator School,
- 1487 Jyvaskyla, Finland, 7-18 September 1992
- 1488 13. Méot, F.: Zgoubi Users' Guide.
- 1489 <https://www.osti.gov/biblio/1062013-zgoubi-users-guide> Sourceforge latest version:
- 1490 <https://sourceforge.net/p/zgoubi/code/HEAD/tree/trunk/guide/Zgoubi.pdf>